Langmuir

Article

pubs.acs.org/Langmuir

Molecular Tailoring of Interfacial Failure

Martha E. Grady,[†,∥] Philippe H. Geubelle,[‡,∥] Paul V. Braun,[§,∥] and Nancy R. Sottos*[,§,∥]

[†]Department of Mechanical Science and Engineering, University of Illinois at Urbana-Champaign, 1206 W. Green Street, Urbana, Illinois 61801, United States

[‡]Department of Aerospace Engineering, University of Illinois at Urbana-Champaign, 104 S. Wright Street, Urbana, Illinois 61801, United States

[§]Department of Materials Science and Engineering, University of Illinois at Urbana-Champaign, 1304 W. Green Street, Urbana, Illinois 61801, United States

[∥]Beckman Institute for Advanced Science and Technology, 405 N. Mathews Avenue, Urbana, Illinois 61801, United States

Supporting Information

ABSTRACT: Self-assembled monolayers (SAMs) provide an enabling platform for molecular tailoring of the chemical and physical properties of an interface. In this work, we systematically vary SAM end-group functionality and quantify the corresponding effect on interfacial failure between a transfer printed gold (Au) film and a fused silica substrate. SAMs with four different end groups are investigated: 11-amino-undecyltriethoxysilane (ATES), dodecyltriethoxysilane (DTES), 11-bromo-undecyltrimethoxysilane (BrUTMS), and 11-mercapto-undecyltrimethoxysilane (MUTMS). In addition to these four end groups, mixed monolayers of increasing molar ratio of MUTMS to DTES in solution are investigated. The failure of each SAM-mediated interface is initiated by a noncontact laser-induced spallation method at strain rates in excess of 10^6 s^{-1}. By making multiple measurements at increasing stress amplitudes (controlled by the laser fluence), we measure interface strengths of 19 ± 1.7, 20 ± 1.3, 52 ± 5.4, and 80 ± 6.5 MPa for interfaces functionalized with ATES, DTES, BrUTMS, and MUTMS, respectively. The interface strength is effectively tuned between the low strength of DTES and the high strength of MUTMS by controlling the concentration of MUTMS in solution. X-ray photoelectron spectroscopy of the failed interfaces reveals the influence of end group functionality on molecular dissociation, which significantly alters the failure process.

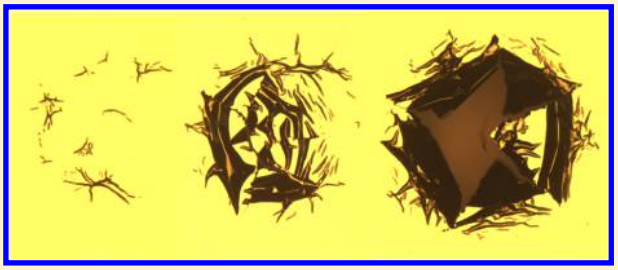

1. INTRODUCTION

The mechanical properties of SAM-modified interfaces have been investigated by both macroscale fracture testing and by more localized scanning probe techniques where tip, sample, or both surfaces are functionalized with SAMs. Both interfacial force microscopy and atomic force microscopy have been employed to investigate adhesive forces with SAM-functionalized constituents.[1−14] Bush et al. measured the elastic modulus, work of adhesion, and interfacial shear strength of methyl-terminated alkylsilane SAMs through scanning probe normal and lateral force measurements.[1] Houston and Kim measured differences in frictional behavior of alkanethiol monolayers due to different end group chemistries and chain lengths.[2−5] Wang and Liechti developed a protocol to form monolayers with nanoscale uniformity, used an interfacial force microscope to measure adhesion of SAM-modified interfaces, and also examined the nonlinear behavior of the SAM.[6−8]

The prospect of using SAMs to modulate bonding in thin film components requires testing of larger contact areas. At the macroscopic scale, the influence of several self-assembled monolayer chemistries on interface adhesion has been investigated using the superlayer test method,[15] fiber pull out method,[16] tape peel test,[17] four-point-bend method,[18,19] and other sandwich specimen configurations.[20−26] Zhuk et al. adapted a superlayer test configuration to measure the strength of an Au−epoxy interface.[15] An increase in fracture energy was measured with incorporation of higher fractions of methyl/epoxy bonds to COOH/epoxy bonds. Mello et al. used a biaxial loading device to perform mixed-mode facture experiments on SAM-mediated epoxy−sapphire interfaces.[24] They reported an increase in interfacial fracture toughness for sapphire surfaces functionalized with bromine-terminated SAMs over surfaces with methyl-terminated SAMs. Gandhi et al. used the four-point-bend method to measure increased interfacial fracture toughness of a SAM-modified Cu−Si interface after thermal annealing.[27] In all of these macroscopic tests, the fracture energy was highly sensitive to SAM composition at the interface of interest.

In this work, the effect of end-group chemistry on the failure process of the SAM-mediated interface is characterized by a laser-induced spallation protocol at strain rates in excess of 10^6 s^{-1}.[28−34] The benefits of laser-induced spallation methods are noncontact stress wave generation, high strain rates, applicability to both tough and weak interfaces, and the ability to test

Received: June 10, 2014
Revised: August 18, 2014
Published: August 25, 2014

multiple sites on the same specimen. The duration of the loading is on the order of nanoseconds, which begins to approach the time scale of molecular dynamics simulations.[35−38] Interestingly though, the SAM-modified interfaces investigated previously by Wang et al.[6−8] and Mello et al.[24] under quasi-static conditions had interface strengths comparable to the strengths found in this study.

The interfacial strength is measured for an Au film transfer-printed to a self-assembled monolayer (SAM) functionalized fused silica substrate (Figure 1). The SiO_2/Au interface was

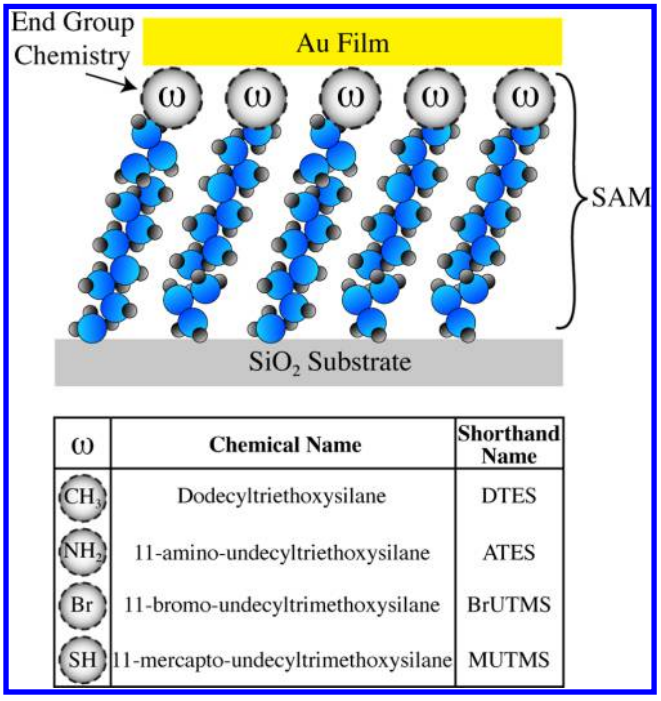

ω	Chemical Name	Shorthand Name
CH_3	Dodecyltriethoxysilane	DTES
NH_2	11-amino-undecyltriethoxysilane	ATES
Br	11-bromo-undecyltrimethoxysilane	BrUTMS
SH	11-mercapto-undecyltrimethoxysilane	MUTMS

Figure 1. Schematic of Au film transfer-printed on SAM-functionalized substrate and the different end group chemistries investigated.

chosen because bifunctional SAM molecules with orthogonal attachment chemistries having specificity toward either SiO_2 or Au can be investigated. The end-group functionality controls the bond strength across the SiO_2/Au interface. Silane chemistries on the silica surface permit dense packing and strong bonding. Four different termination chemistries (−CH_3, −NH_2, −Br, −SH) shown schematically in Figure 1 were selected to obtain a large variation in bond strength at the Au−SAM interface. Mixed monolayers of increasing molar ratio of −SH to −CH_3 in solution were also prepared. When properly formed, these chemistries do not result in multilayer formation or loop attachment to the fused silica substrate. Previous work in molecular electronics has demonstrated that the "soft-deposition" approach of transfer printing, as compared to more energetic physical vapor deposition techniques, causes minimal damage to the SAM layer.[39] Because adhesion between the elastomeric stamp and Au film is dominated by peel rate, Au layers can be transfer-printed to a variety of functionalized surfaces.[40]

EXPERIMENTAL SECTION

Materials. The fused silica substrates (SiO_2, 1500 μm thick, Quartz Scientific) were cleaned in piranha solution (3 H_2SO_4:1 H_2O_2 by volume) at 120 °C for 60 min. The substrates were then rinsed with copious amounts of water, dried under a stream of air, and further dried in an oven at 120 °C for at least 5 min. In addition, silicon wafers (University Wafer) with a native oxide layer were diced to 1 cm^2 and were prepared in the same manner for ellipsometry measurements. SAMs were formed on both fused silica and silicon substrates in the same reaction vessel by immersion in a toluene solution (ACS certified, Fisher Scientific) of 10 mM silane (11-amino-undecyltriethoxysilane (ATES), dodecyltriethoxysilane (DTES), 11-bromo-undecyltrimethoxysilane (BrUTMS), and 11-mercapto-undecyltrimethoxysilane (MUTMS)) plus 15 mM triethylamine for 24 h in a sealed container on the benchtop. We found that anhydrous solvents and preparation in an inert atmosphere did not improve monolayer formation for alkoxysilanes.[41] All SAM deposition procedures followed the above protocols, however, the results of a time in solution study for amine-terminated monolayers demonstrated that only 1 h was necessary for full coverage and formation of a single monolayer without the addition of a triethylamine catalyst. Additionally, 0.03 g of dithiothreitol (Sigma-Aldrich) was added to solutions with thiols to reduce disulfide formation. SAM layer thicknesses of 10−13 Å were confirmed using a Gaertner ellipsometer. Samples were also prepared with mixed monolayers containing a range of MUTMS to DTES mole percents of each SAM molecule in solution. The MUTMS mole fractions used in these experiments were 0, 25, 50, 75, and 100%, which corresponds to a fully thiol-terminated SAM (MUTMS). X-ray photoelectron spectroscopy was used to validate the presence of thiol molecules at the surface by distinguishing a signal from the sulfur 2s orbital following the protocol developed by Losego et al. to confirm mixed monolayer concentrations.[41]

After rinsing (subsequent rinses of toluene, ethanol, and deionized water) and drying, a thin Au layer was transfer-printed onto the SAM-functionalized substrate following the procedures of Meitl et al.[40] Donor silicon substrates with thermally grown oxide layers (~75 nm) were cleaned in a piranha solution, rinsed with deionized water, and blown dry. Gold films of nominally 150 nm thickness were deposited by e-beam evaporation (Temescal) onto the Si/SiO_2 donor substrates. Poor adhesion at the SiO_2/Au interface makes these oxide surfaces ideal donor substrates for the transfer printing process. A thin layer of poly(vinyl alcohol) (PVA) (87-89% hydrolyzed, MW ~ 20 000 g/mol, Sigma-Aldrich, 10 wt % dissolved in H_2O) was cast onto the Au surface to impart mechanical stability during the transfer process. The PVA layer was dried at 85 °C for 5 min. A block (approx. 2 cm × 2 cm × 0.7 cm thick) of polydimethylsiloxane (PDMS, Sylgard 184 Silicon Elastomer, Dow-Corning) was used to transfer the film. The PDMS was manually pressed onto the donor substrate such that it completely conformed to the Au/PVA surface. The stamp was then rapidly peeled, causing delamination and resulting in the PDMS stamp being "inked" with the gold film. The film was laminated to the receiving, prefunctionalized fused silica substrate and heated on a hot plate at 110 °C. After 90 s of manual pressure, the PDMS stamp was slowly peeled from the surface leaving the Au/PVA film bonded to the substrate. The specimen was kept on the hot plate for another 90 s to finish bonding. The PVA layer was then rinsed away under flowing water. After transfer printing the Au film onto the functionalized substrates, specimens were prepared for laser spallation testing (Figure 2). A 400 nm thick Al absorbing layer was e-beam evaporated on to the backside followed by spin-casting a 1 μm sodium silicate (waterglass) confining layer. Specimens for stress wave calibration were fabricated with highly reflective thin Al films (200 nm) that were electron-beam deposited on identical substrates as SAM/Au specimens.

Laser Spallation. The laser spallation method, shown schematically in Figure 2, was used to load the SAM-functionalized interface in a noncontact manner. A rapid (~10 ns), high-amplitude acoustic wave was initiated by the impingement of an Nd:YAG pulsed laser (New Wave Tempest) on the aluminum energy absorbing layer on the back surface of the substrate. Because of the confinement of a sodium silicate (waterglass) layer, the rapid expansion of the Al generated an acoustic wave that propagated through the substrate in compression. After reflection at the thin film free surface, the wave loaded the thin film−substrate interface in tension. The Nd:YAG spot size was kept constant at 2.0 mm for all tests and the laser fluence (energy per area) was incremented by adjusting the Nd:YAG energy using an attenuation controller. Specimens were tested over a range of

dx.doi.org/10.1021/la502271k | Langmuir 2014, 30, 11096−11102

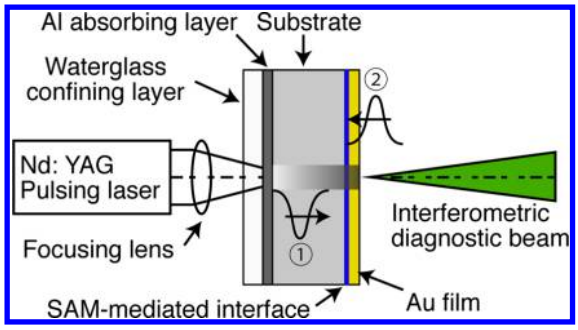

Figure 2. Schematic of test configuration for generation of high amplitude stress waves in SAM-mediated transfer-printed Au films. A compressive stress pulse ① propagates toward the film. After reflection at the free surface, the tensile stress pulse ② loads the SAM-mediated interface in tension.

laser fluences (energy per area) to initiate delamination of the Au film. A single specimen was tested multiple times by using motion-controlled actuators to move to a new location 1.5 times the spot size from the center of the previous site. After testing, the films were evaluated for damage using an optical microscope.

The interfacial strength of SAM-mediated interfaces was measured by determining the stress required to cause film failure at the interface. Calibration experiments with highly reflective thin Al films were carried out to obtain the substrate and interface stresses for a given laser fluence (energy per area). A calibration set was necessary because the SiO_2/SAM/Au films partially failed at laser fluences of interest, precluding in situ interferometry measurements. Repeatable acoustic waves were generated at the same laser fluence in both types of samples. The displacement of the free surface and corresponding substrate stress was recorded as described previously by Grady et al.[42] Using the measured stress pulses as input for a 1D finite element model, the interface stress was calculated over a range of fluences for 150 nm thick Au films on fused silica substrates. The difference in thickness and stiffness between the Al calibration films and the Au films was accounted for in the stress calculations. Details of the stress analysis are provided in the Supporting Information.

Atomic Force Microscopy. Atomic force microscopy (AFM) was used to investigate the nanoscale surface of SAM-functionalized substrates as well as Au films. AFM was conducted in tapping mode using an Asylum Research Cypher system to provide surface height information, from which a root-mean-square (RMS) surface roughness was calculated. The surface roughness was measured on a MUTMS-functionalized fused silica surface, a MUTMS-functionalized silicon surface, and on the mating surface of a transfer-printed Au film. The Au film was removed from the donor substrate and the mating surface of the Au film was turned upright for scanning with the AFM.

X-ray Photoelectron Spectroscopy. A Kratos Axis Ultra X-ray Photoelectron Spectroscope was used to provide surface chemical information within the debonded regions and to compare spectra to a fully formed SAM. High-resolution spectra were collected using monochromatic Al Ka radiation (1486.6 eV) with a pass energy of 40 eV from a 0.2 mm diameter area within the spalled region. The binding energy scale was referenced to the adventitious C 1s signal at 285 eV. Peaks on an XPS spectra signaling the presence of sulfur atoms within the MUTMS SAMs are expected to be centered at 228 eV corresponding to the 2s orbital and peaks signaling the presence of bromine atoms within the BrUTMS SAMs are expected to be centered around 71 eV corresponding to the 3d orbital. After accounting for differences in relative sensitivity, the peak area of these spectral lines indicate relative amounts of elements present on the surface. The XPS spectra obtained in the debonded portion of a tested specimen were compared to a clean unmodified fused silica substrate and a pristine SAM on fused silica.

RESULTS AND DISCUSSION

Interfacial Strength. Thin film specimens prepared with 11-amino-undecyltriethoxysilane (ATES), dodecyltriethoxysilane (DTES), 11-bromo-undecyltrimethoxysilane (BrUTMS), and 11-mercapto-undecyltrimethoxysilane (MUTMS) at the interface between fused silica substrates and transfer-printed Au films were tested at increasing laser fluences using the laser spallation technique shown in Figure 2. Specimens were also prepared with mixed monolayers containing a range of MUTMS to DTES mole percents of each SAM molecule in solution. After testing, loaded regions of the SiO_2/SAM/Au specimens were examined by optical microscopy. Figure 3 contains representative

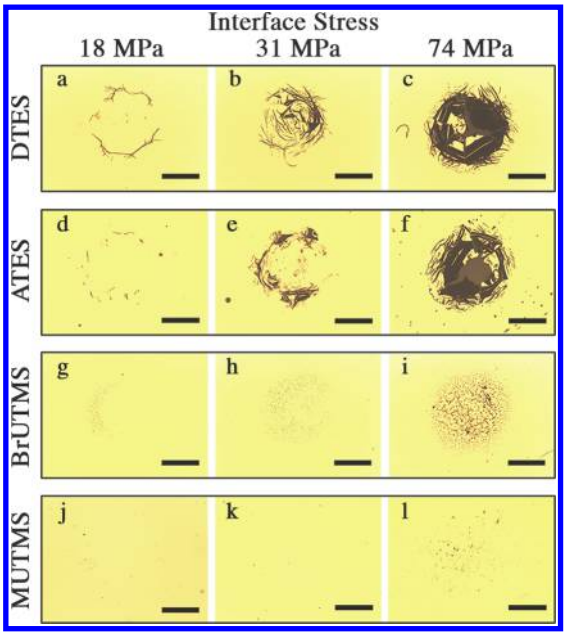

Figure 3. Optical images of film failure (black areas) caused by laser spallation to (a–c) DTES interfaces, (d–f) ATES, (g–i) BrUTMS, and (j–l) MUTMS interfaces at increasing stress amplitudes: (a,d,g,j,) 18 MPa, (b,e,h,k) 31 MPa, and (c,f,i,l) 74 MPa. Scale bars are 500 μm.

images of Au films tested at increasing interfacial stress for each of the four different SAMs investigated. Tensile stresses on the interface caused the film to detach from the substrate. Black areas in the optical images correspond to spalled regions where the Au film has separated from the substrate. Onset of film failure occurred at lower interfaces stresses for ATES and DTES than BrUTMS and MUTMS. The size of failed regions increased with increased stress levels until reaching the Nd:YAG laser spot size. The effect of mixed monolayers at the interface was also investigated. Representative images of Au films after laser spallation testing with corresponding interfacial stress loading for different molar ratios of MUTMS in solution: 0 (DTES), 25, 50, 75, and 100% (MUTMS) are included in the Supporting Information.

Film failure initiated over a range of interface stress levels. Failure observations for each specimen type are summarized in Figure 4, which shows the fraction of films that exhibit failure at a given peak interface stress. The fraction plotted in Figure 4 represents the number of films that failed divided by the number tested at the same peak interface stress. For example in Figure 4a, at a peak interface stress of 31 MPa, 0% of MUTMS specimens failed, 44% of BrUTMS specimens failed, and 100% of the DTES and ATES specimens failed. Figure 4b shows the failure data for FS/SAM/Au specimens with mixed monolayer SAMs: 0 (DTES), 25, 50, 75, and 100% (MUTMS). Over 750 film sites were tested across the seven interfacial chemistries and eight interface stress loading conditions. The number of tests in the range of interest for each chemistry was always greater than or

dx.doi.org/10.1021/la502271k | Langmuir 2014, 30, 11096–11102

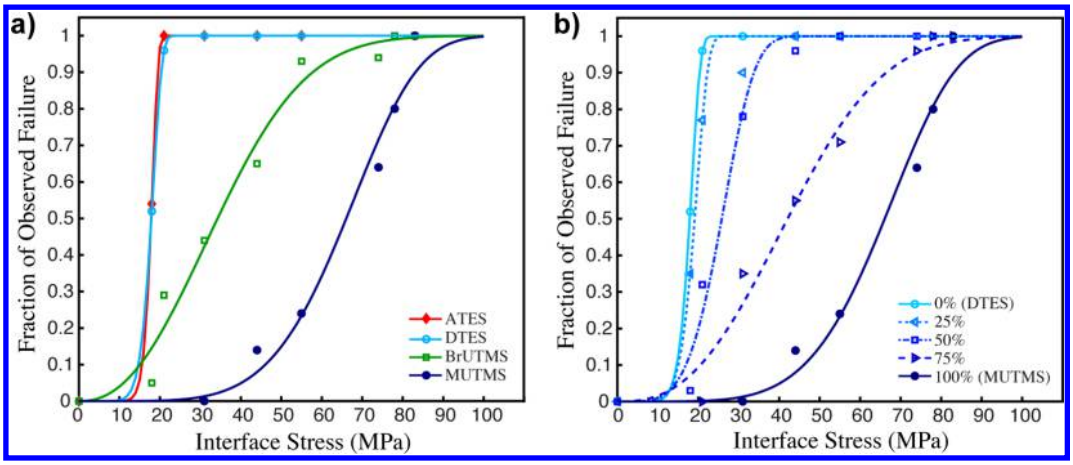

Figure 4. Fraction of testing sites that showed delamination for FS/SAM/Au interfaces as a function of calibrated interface stress for (a) ATES, DTES, BrUTMS, MUTMS and (b) mixed monolayers of MUTMS to DTES in solution at 0, 25, 50, 75, and 100% concentrations. Experimental data is represented by symbols and the associated Weibull curve fit is plotted for each SAM.

equal to 10. The failure stress data for each specimen type was fit to a Weibull distribution[43]

$$F(\sigma) = 1 - e^{-(\frac{\sigma}{\alpha})^{\beta}} \quad (1)$$

where σ is peak interface stress and α and β are Weibull parameters. The Weibull parameters varied for each SAM type and are included in Table 1.

Table 1. Interface Strength for Each SAM, Uncertainty, Corresponding Weibull Parameters, and Root Mean Square (RMS) Difference between Model and Experimental Data

SAM	strength (μ + σ_{sd}) MPa	strength uncertainty MPa	α parameter	β parameter	RMS
ATES	19	1.7	18.31	14.82	.000200
DTES	20	1.3	18.59	9.59	.000002
25%	22	1.0	20.01	7.96	.040825
50%	32	1.9	28.00	4.48	.047183
75%	61	6.2	48.28	2.65	.055046
MUTMS	80	6.5	70.85	5.22	.057559
BrUTMS	52	5.4	40.18	2.30	.053782

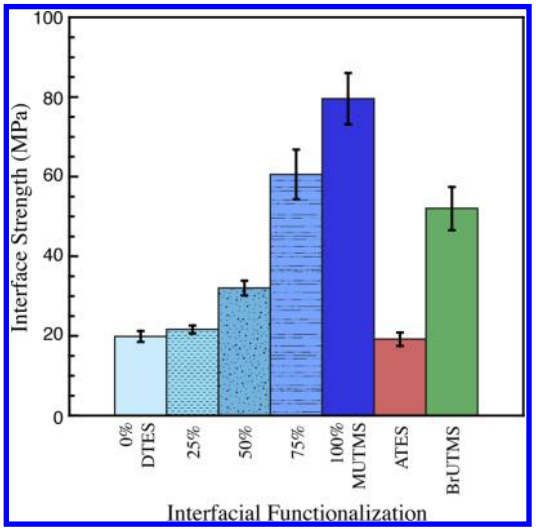

Figure 5. Interface strength of all SAMs investigated. The error bars represent the uncertainty in the Weibull fit arising from experimental error.

Both the onset of interfacial failure and 100% failure occur at higher stresses for the MUTMS/Au as compared to both ATES/Au and DTES/Au, confirming the stronger bonding at the thiol-Au interface. The BrUTMS/Au interface exhibited a failure strength between DTES/Au and MUTMS/Au interfaces. One possibility is that the heavier Bromine moiety induces stronger van der Waals forces than either a methyl or an amine moiety thus leading to higher interfacial strength.[44] For mixed monolayers of DTES and MUTMS, the onset of film failure occurred at higher interface stresses with increased incorporation of thiol-terminated SAMs.

The interface strength was determined by calculating the mean and standard deviation, μ + σ_{sd}, of the Weibull model corresponding to an approximate failure rate of 85−90%. The interfacial strengths for all of the SAMs investigated are plotted in Figure 5 and summarized in Table 1. We calculate interfacial strengths of 19 ± 1.7, 20 ± 1.3, 52 ± 5.4, and 80 ± 6.5 MPa for interfaces prepared with ATES, DTES, BrUTMS, and MUTMS, respectively. The interface strengths for 25, 50, and 75% MUTMS monolayers were 22 ± 1.0, 32 ± 1.9, and 61 ± 6.2 MPa, respectively. As expected, increased incorporation of MUTMS SAMs in mixed monolayers resulted in increased interfacial strength.

Surface Roughness. The effect of substrate roughness was also examined for the MUTMS/Au interface. Interface strength was measured as described previously for this SAM on a polished silicon wafer. Silicon substrates have a significantly reduced surface roughness and provide a SiO_2 surface for SAM functionalization. The surface roughnesses of bare substrates, SAM-functionalized substrates, and transfer-printed Au films were measured by atomic force microscopy (AFM). Representative 1 × 1 μm AFM scans are included in Figure 6 for FS/MUTMS, Si/MUTMS, and the underside of an Au film. The RMS roughness is calculated over the entire surface shown in Figure 6 yielding roughness values of 7.4, 1.2, and 2.7 Å for MUTMS-functionalized fused silica, MUTMS-functionalized silicon, and the underside of Au, respectively. For comparison, a subset of a single line trace indicated by white arrows is plotted in Figure 6d for the three surfaces. Typically, AFM on physical vapor deposition (PVD) films reveals distinct grain sizes, however, the underside of the film did not reveal the same morphology as the surface.

dx.doi.org/10.1021/la502271k | Langmuir 2014, 30, 11096−11102

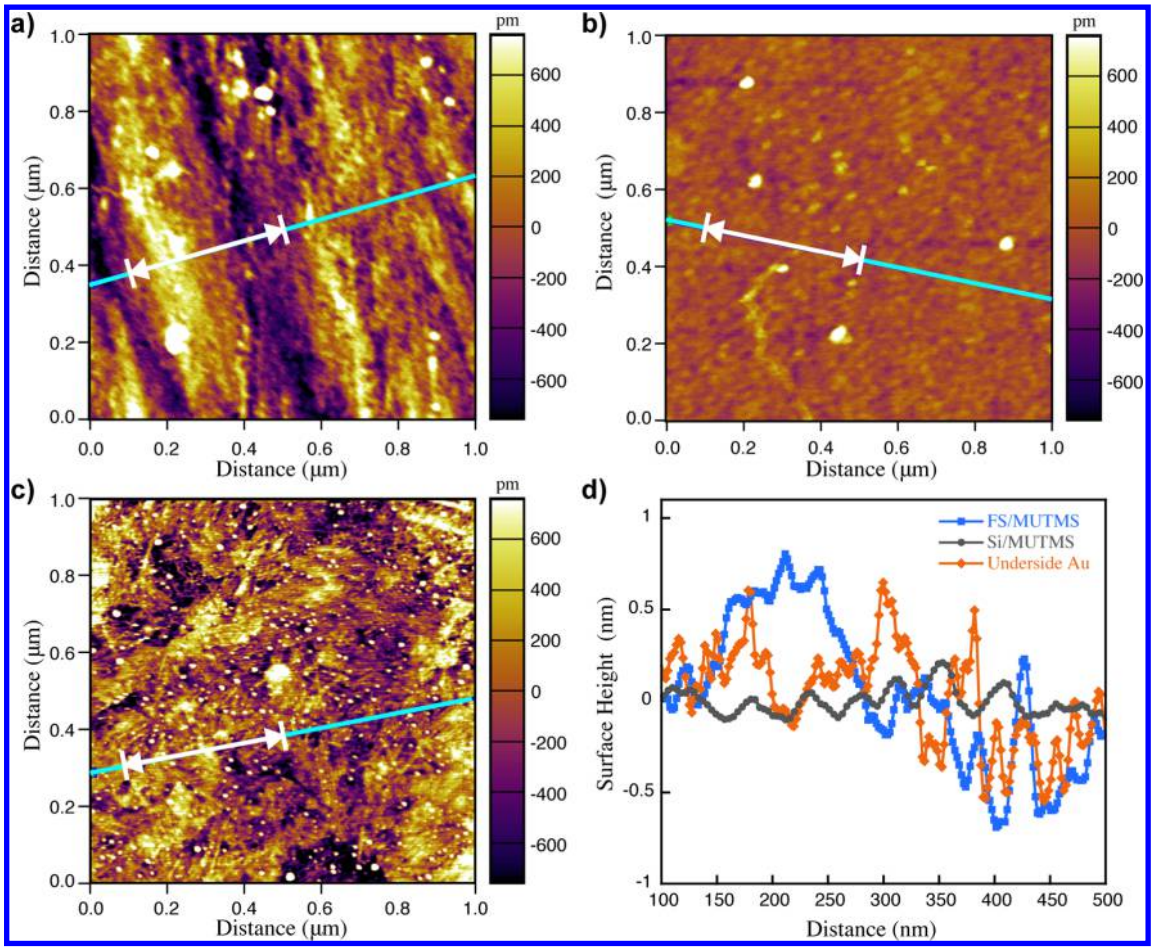

Figure 6. AFM scans are shown for (a) MUTMS-functionalized fused silica substrate, (b) MUTMS-functionalized silicon substrate, (c) underside of an Au transfer-printed film, and (d) subset of the line trace indicated by white arrows (a–c) demonstrating the large difference in surface roughness between functionalized fused silica and silicon substrates.

Polished silicon wafers were functionalized with MUTMS and Au films (150 nm) were transfer printed following the previously described protocol. The films were loaded by incrementing the laser fluence and calibration experiments were performed to obtain the interface stress at each laser fluence. Optical microscopy was used to investigate the loaded regions of the Si/MUTMS/Au samples and the interface stress required to delaminate the Au film from the MUTMS-functionalized silicon substrate was over 200 MPa. Remarkably, the interface strength of these films was 250% greater than for MUTMS-functionalized fused silica substrates. Our hypothesis is that the rougher fused silica surface did not allow as much contact between the SAM and the Au film limiting the likelihood for covalent bonds to form between the thiol and the Au film. Conversely, the smoother silicon surface may have allowed a higher density of covalent bonds to form between the thiol and Au film due to more intimate contact. The higher density of covalent bonds between the SAM and the Au film results in increased interface strength.

X-ray Photoelectron Spectroscopy of Failed Interfaces. At high laser fluences, the Au film completely separates from the surface exposing the underlying interfacial SAM layer. The debonded portion is approximately circular with a diameter greater than 0.5 mm. Positioning of the X-ray beam within the debonded portion is accomplished using imaging mode where the signal from the gold layer is strong and can be observed in real time on the surface. The center of the X-ray beam is then aligned within the failed region, which appears dark. The chemical composition of these failed SAM interfaces was investigated using X-ray photoelectron spectroscopy (XPS). The XPS spectra obtained in the debonded portion of a tested specimen were compared to a bare fused silica substrate and a pristine SAM on fused silica for BrUTMS and MUTMS (Figure 7). Spectra peaks signaling the presence of bromine atoms within the BrUTMS SAMs are expected to be centered around 71 eV as shown for a pristine BrUTMS SAM in Figure 7a. There is a significant difference in peak height between the spectra for the pristine BrUTMS monolayer and the spectra from debonded regions. Five separate debonded regions of BrUTMS-functionalized interfaces were probed for surface chemical information and are overlaid in Figure 7a. As expected, there are no signal peaks within this region for the unmodified fused silica substrate. The characteristic peak signaling the presence of sulfur atoms within the MUTMS SAMs is expected to be centered at 228 eV. The spectra from debonded regions for specimens with interfacial MUTMS SAMs showed a less dramatic change in peak height from a pristine monolayer shown in Figure 7b. Five separate debonded regions of MUTMS-functionalized interfaces were probed for surface chemical information and are overlaid in Figure 7b. The debonded regions of MUTMS-functionalized interfaces have highly repeatable spectra signaling sulfur atoms are present on the surface after testing. One hypothesis for the difference in peak signal between the surface control monolayers and within spalled regions is that the rapid debonding of the Au film during laser spallation testing could be inducing local

dx.doi.org/10.1021/la502271k | *Langmuir* 2014, 30, 11096–11102

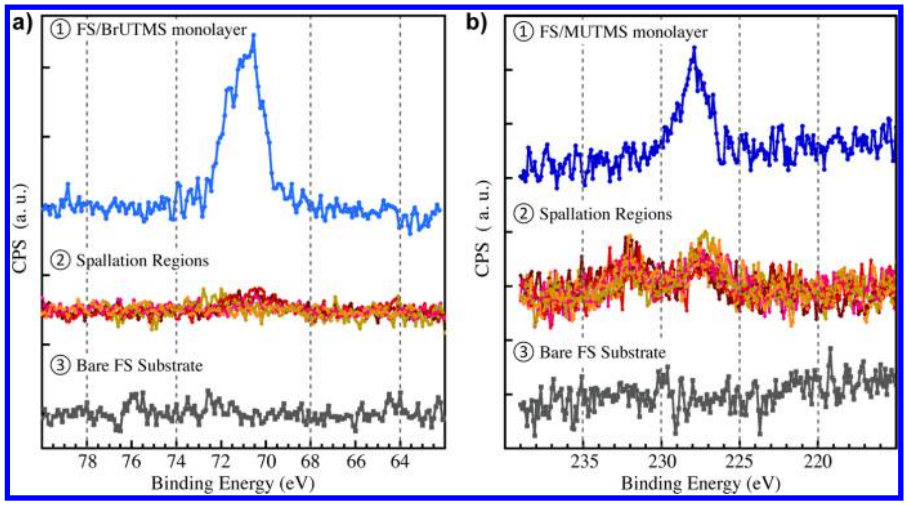

Figure 7. (a) XPS spectra for ① BrUTMS-functionalized substrate, ② five separate debonded regions, and ③ bare FS substrate. (b) XPS spectra for ① MUTMS-functionalized substrate, ② five separate debonded regions, and ③ bare FS substrate.

molecular failure where the terminating moiety is expelled from the surface. The recovery of spalled Au films was not possible and therefore XPS could not be performed to identify the presence of the terminating moiety on the films as a complement to the debonded regions. The XPS characterization of failed MUTMS/Au and BrUTMS/Au interfaces revealed the possibility of local SAM failure due to rapid stress wave loading.

CONCLUSIONS

The adhesion of a SAM-mediated interface between transfer-printed Au films and a fused silica substrate was measured by a laser spallation technique. Different SAM termination chemistries of amine, methyl, bromine, thiol, and mixed monolayers were investigated. Specimens were tested at increasing laser fluence, which corresponded to increasing interface stress. Interfacial failure was statistical in nature and fit well to a Weibull distribution. Thiol-terminated SAMs led to the strongest interface, while both the amine- and methyl-terminated SAMs resulted in the weakest interfacial strength. Interestingly, the interface strength of specimens with bromine-terminated SAMs was midway between that of the methyl and thiol SAMs. The use of mixed monolayers provided a more systematic way to vary interfacial strength. The interfacial failure process is effectively controlled through the choice of SAM termination chemistry. In addition to the chemical functionality of the SAM, surface roughness of the underlying substrate also has a significant impact on the interfacial strength. Decreasing the substrate surface roughness increased the contact area between the thiol-terminated SAM and the Au film leading to an increase in interfacial strength. XPS analysis within debonded regions revealed a difference in signal from pristine monolayers on the same substrate indicating the possibility of local monolayer failure.

ASSOCIATED CONTENT

Supporting Information

Interfacial stress calculations, loading of MUTMS-functionalized silicon, optical images of failed interfaces, and Weibull parameters. This material is available free of charge via the Internet at http://pubs.acs.org.

AUTHOR INFORMATION

Corresponding Author

*E-mail: n-sottos@illinois.edu. Address: 405 N. Mathews M/C 251 Urbana, IL 61801.

Author Contributions

The manuscript was written through contributions of all authors. All authors have given approval to the final version of the manuscript.

Notes

The authors declare no competing financial interest.

ACKNOWLEDGMENTS

The authors gratefully acknowledge support from NSF CMMI 11-61517. The authors also thank the Beckman Institute for Advanced Science and Technology for their assistance in this work. Experiments were carried out in part in the Frederick Seitz Materials Research Laboratory Central Research Facilities, University of Illinois. We specifically acknowledge Richard Haasch for his expertise and assistance with X-ray photoelectron spectroscopy.

ABBREVIATIONS

Nd:YAG, neodymium-doped yttrium aluminum garnet; SAM, self-assembled monolayer; PVA, poly(vinyl alcohol); PDMS, polydimethylsiloxane; PVD, physical vapor deposition; MD, molecular dynamics

REFERENCES

(1) Bush, B. G.; Del Rio, F. W.; Jaye, C.; Fischer, D. A.; Cook, R. F. Interfacial Mechanical Properties of n-Alkylsilane Monolayers on Silicon Substrates. *J. Microelectromech. Syst.* **2013**, *22*, 34−43.

(2) Houston, J. E.; Doelling, C. M.; Vanderlick, T. K.; Hu, Y.; Scoles, G.; Wenzl, I.; Lee, T. R. Comparative Study of the Adhesion, Friction, and Mechanical Properties of CF3- and CH3-Terminated Alkanethiol Monolayers. *Langmuir* **2005**, *21*, 3926−3932.

(3) Houston, J. E.; Kim, H. I. Adhesion, friction, and mechanical properties of functionalized alkanethiol self-assembled monolayers. *Acc. Chem. Res.* **2002**, *35*, 547−553.

(4) Kim, H. I.; Houston, J. E. Separating Mechanical and Chemical Contributions to Molecular-Level Friction. *J. Am. Chem. Soc.* **2000**, *122*, 12045−12046.

(5) Kim, H. I.; Boiadjiev, V.; Houston, J. E.; Zhu, X. Y.; Kiely, J. D. Tribological properties of self-assembled monolayers on Au, SiOx and Si surfaces. *Tribol. Lett.* **2001**, *10*, 97−101.
(6) Wang, M. J.; Liechti, K. M.; White, J. M.; Winter, R. M. Nanoindentation of polymeric thin films with an interfacial force microscope. *J. Mech. Phys. Solids* **2004**, *52*, 2329−2354.
(7) Wang, M. J.; Liechti, K. M.; Wang, Q.; White, J. M. Self-Assembled Silane Monolayers: Fabrication with Nanoscale Uniformity. *Langmuir* **2005**, *21*, 1848−1857.
(8) Wang, M. J.; Liechti, K. M.; Srinivasan, V.; White, J. M.; Rossky, P. J.; Stone, M. T. A hybrid continuum-molecular analysis of interfacial force microscope experiments on a self-assembled monolayer. *J. Appl. Mech.* **2006**, *73*, 769−777.
(9) Chandross, M.; Webb, E. B.; Stevens, M. J.; Grest, G. S.; Garofalini, S. H. Systematic study of the effect of disorder on nanotribology of self-assembled monolayers. *Phys. Rev. Lett.* **2004**, *93*, 166103.
(10) Kiely, J. D.; Houston, J. E.; Mulder, J. A.; Hsung, R. P.; Zhu, X. Y. Adhesion, deformation and friction for self-assembled monolayers on Au and Si surfaces. *Tribol. Lett.* **1999**, *7*, 103−107.
(11) DelRio, F. W.; Jaye, C.; Fischer, D. A.; Cook, R. F. Elastic and adhesive properties of alkanethiol self-assembled monolayers on gold. *Appl. Phys. Lett.* **2009**, *94*, 131909.
(12) Lee, D. H.; Kim, D.; Oh, T.; Cho, M. Phase State Effect on Adhesion Behavior of Self-Assembled Monolayers. *Langmuir* **2004**, *20*, 8124−8130.
(13) Xu, C.; Jones, R. L.; Batteas, J. D. Dynamic variations in adhesion of self-assembled monolayers on nanoasperities probed by atomic force microscopy. *Scanning* **2008**, *30*, 106−117.
(14) Yang, Y. T.; Jamison, A. C.; Barriet, D.; Lee, T. R.; Ruths, M. Odd-Even Effects in the Friction of Self-Assembled Monolayers of Phenyl-Terminated Alkanethiols in Contacts of Different Adhesion Strengths. *J. Adhes. Sci. Technol.* **2010**, *24*, 2511−2529.
(15) Zhuk, A. V.; Evans, A. G.; Hutchinson, J. W.; Whitesides, G. M. The adhesion energy between polymer thin films and self-assembled monolayers. *J. Mater. Res.* **1998**, *13*, 3555−3564.
(16) Feresenbet, E.; Raghavan, D.; Holmes, G. A. The role of the terminal functional group of self-assembled monolayers on fiber matrix adhesion. *J. Appl. Polym. Sci.* **2007**, *106*, 462−469.
(17) Zou, L.; De Guire, M.; Wang, R. Effect of organic self-assembled monolayers on the deposition and adhesion of hydroxyapatite coatings on titanium. *Int. J. Mater. Res.* **2006**, *97*, 760−767.
(18) Caro, A. M.; Armini, S.; Richard, O.; Maes, G.; Borghs, G.; Whelan, C. M.; Travaly, Y. Bottom-Up Engineering of Subnanometer Copper Diffusion Barriers Using NH_2-Derived Self-Assembled Monolayers. *Adv. Funct. Mater.* **2010**, *20*, 1125−1131.
(19) Jang, E. J.; Park, Y. B.; Lee, H. J.; Choi, D. G.; Jeong, J. H.; Lee, E. S.; Hyun, S. Effect of surface treatments on interfacial adhesion energy between UV-curable resist and glass wafer. *Int. J. Adhes. Adhes.* **2009**, *29*, 662−669.
(20) Kent, M. S.; Reedy, E. D.; Yim, H.; Matheson, A.; Sorenson, J.; Hall, J.; Schubert, K.; Tallant, D.; Garcia, M.; Ohlhausen, T.; Assink, R. Using self-assembling monolayers to study crack initiation in epoxy/silicon joints. *J. Mater. Res.* **2004**, *19*, 1682−1695.
(21) Kent, M. S.; Yim, H.; Matheson, A.; Cogdill, C.; Nelson, G.; Reedy, E. D. Use of self-assembled monolayers at variable coverage to control interface bonding in a model study of interfacial fracture: Pure shear loading. *J. Adhes.* **2001**, *75*, 267−298.
(22) Kinloch, A. J.; Tan, K. T.; Watts, J. F. Novel self-assembling silane for abhesive and adhesive applications. *J. Adhes.* **2006**, *82*, 1117−1132.
(23) Liechti, K. M.; Na, S. R.; Wakamatsu, M.; Seitz, O.; Chabal, Y. A High Vacuum Fracture Facility for Molecular Interactions. *Exp. Mech.* **2013**, *53*, 231−241.
(24) Mello, A. W.; Liechti, K. M. A piezoelectric biaxial loading device for interfacial fracture experiments. *Exp. Mech.* **2004**, *44*, 495−501.
(25) Mello, A. W.; Liechti, K. M. The effect of self-assembled monolayers on interfacial fracture. *J. Appl. Mech.* **2006**, *73*, 860−870.
(26) Smith, J. W.; Kramer, E. J.; Mills, P. J. Tailored Adhesion at Polymer Nonpolymer Interfaces. *J. Polym. Sci., Part B: Polym. Phys.* **1994**, *32*, 1731−1744.
(27) Gandhi, D. D.; Lane, M.; Zhou, Y.; Singh, A. P.; Nayak, S.; Tisch, U.; Eizenberg, M.; Ramanath, G. Annealing-induced interfacial toughening using a molecular nanolayer. *Nature* **2007**, *447*, 299−303.
(28) Gupta, V.; Argon, A. S.; Cornie, J. A.; Parks, D. M. Measurement of Interface Strength by Laser-Pulse-Induced Spallation. *Mater. Sci. Eng., A* **1990**, *126*, 105−117.
(29) Gupta, V.; Argon, A. S.; Parks, D. M.; Cornie, J. A. Measurement of Interface Strength by a Laser Spallation Technique. *J. Mech. Phys. Solids* **1992**, *40*, 141−180.
(30) Gupta, V.; Yuan, J. Measurement of Interface Strength by the Modified Laser Spallation Technique. II. Applications to Metal-Ceramic Interfaces. *J. Appl. Phys.* **1993**, *74*, 2397−2404.
(31) Gupta, V.; Yuan, J.; Pronin, A. Recent Developments in the Laser Spallation Technique to Measure the Interface Strength and Its Relationship to Interface Toughness with Applications to Metal-Ceramic, Ceramic-Ceramic and Ceramic Polymer Interfaces. *J. Adhes. Sci. Technol.* **1994**, *8*, 713−747.
(32) Kandula, S. S. V.; Hartfield, C. D.; Geubelle, P. H.; Sottos, N. R. Adhesion strength measurement of polymer dielectric interfaces using laser spallation technique. *Thin Solid Films* **2008**, *516*, 7627−7635.
(33) Stephens, A. W.; Vossen, J. L. Measurement of Interfacial Bond Strength by Laser Spallation. *J. Vac. Sci. Technol.* **1976**, *13*, 38−39.
(34) Wang, J. L.; Weaver, R. L.; Sottos, N. R. A parametric study of laser induced thin film spallation. *Exp. Mech.* **2002**, *42*, 74−83.
(35) Gao, J. P.; Luedtke, W. D.; Landman, U. Friction Control in Thin-Film Lubrication. *J. Phys. Chem. B* **1998**, *102*, 5033−5037.
(36) Heinz, H.; Vaia, R. A.; Farmer, B. L.; Naik, R. R. Accurate Simulation of Surfaces and Interfaces of Face-Centered Cubic Metals Using 12-6 and 9-6 Lennard-Jones Potentials. *J. Phys. Chem. C* **2008**, *112*, 17281−17290.
(37) Luedtke, W. D.; Landman, U. Structure and Thermodynamics of Self-Assembled Monolayers on Gold Nanocrystallites. *J. Phys. Chem. B* **1998**, *102*, 6566−6572.
(38) Ramin, L.; Jabbarzadeh, A. Effect of Load on Structural and Frictional Properties of Alkanethiol Self-Assembled Mono layers on Gold: Some Odd-Even Effects. *Langmuir* **2012**, *28*, 4102−4112.
(39) Loo, Y. L.; Lang, D. V.; Rogers, J. A.; Hsu, J. W. P. Electrical Contacts to Molecular Layers by Nanotransfer Printing. *Nano Lett.* **2003**, *3*, 913−917.
(40) Meitl, M. A.; Zhu, Z. T.; Kumar, V.; Lee, K. J.; Feng, X.; Huang, Y. Y.; Adesida, I.; Nuzzo, R. G.; Rogers, J. A. Transfer printing by kinetic control of adhesion to an elastomeric stamp. *Nat. Mater.* **2006**, *5*, 33−38.
(41) Losego, M. D.; Grady, M. E.; Sottos, N. R.; Cahill, D. G.; Braun, P. V. Effects of chemical bonding on heat transport across interfaces. *Nat. Mater.* **2012**, *11*, 502−506.
(42) Grady, M. E.; Geubelle, P. H.; Sottos, N. R. Interfacial adhesion of photodefinable polyimide films on passivated silicon. *Thin Solid Films* **2014**, *552*, 116−123.
(43) Murthy, D. N. P.; Xie, M.; Jiang, R. *Weibull models*; J. Wiley: Hoboken, NJ, 2004.
(44) Israelachvili, J. N. *Intermolecular and Surface Forces*, 3rd ed.; Academic Press: Burlington, MA, 2011.